Journal of Geoscience and Environment Protection, 2025, 13(8), 102-120
https://www.scirp.org/journal/gep
ISSN Online: 2327-4344
ISSN Print: 2327-4336

Assessing the Indicators of Water Stress in Usangu Agricultural Wetland, Tanzania

Goodluck Masige[1,2*], Alfred Opere[1], Josphat Mulwa[1]

[1]Department Earth and Climate Science, University of Nairobi, Nairobi, Kenya
[2]Department of Civil Engineering, Mbeya University of Science and Technology, Mbeya, Tanzania
Email: *masigeg@gmail.com

How to cite this paper: Masige, G., Opere, A., & Mulwa, J. (2025). Assessing the Indicators of Water Stress in Usangu Agricultural Wetland, Tanzania. *Journal of Geoscience and Environment Protection, 13,* 102-120.
https://doi.org/10.4236/gep.2025.138006

Received: July 9, 2025
Accepted: August 19, 2025
Published: August 22, 2025

Abstract

Wetlands play a critical role in water retention and supply in drainage connected regions. The Usangu wetland ecosystem contributes to recharging the Ruaha River, which is hydrologically connected to the wetland, supporting both ecological balance and agricultural activities in the region. This study analyzes Land Surface Temperature (LST) data from Landsat 8 and 9, employing machine learning techniques to explore temporal relationships with multiple variables, including the NDVI and the SPI. The SPI dataset, derived from NOAA PERSIANN-CDR satellite images, was analysed from 2000 to 2024 using Google Earth Engine (GEE). The precipitation datasets clustered using the K-Means algorithm to identify SPI drought years. Timeseries charts and Seasonal Trend Decomposition by LOESS (STL) statistical tests, conducted using CHIRPS data with 0.05˚ resolution. Historical CMIP6 model precipitation datasets were bias corrected against the CHIRPS reference dataset using linear scaling, which revealed that the raw CMIP6 outputs consistently overestimated precipitation. The corrected data shows severe dry spells in the wetland region with values frequently below 200 mm/month. The SPI analysis identifies drought years in the watershed, which align with periods of below average precipitation. Linear regression of LST data shows a strong positive correlation between the baseline temperature and predicted data, with a correlation coefficient (r) of 0.79. However, the correlation between LST and the Shuttle Radar Topography Mission Digital Elevation Model (SRTDEM) dataset reveals a negative relationship. This suggests that lower elevations in the wetland experience higher temperatures. LST influences various spectral indices in the wetland. The Water in Wetland (WIW) method detects water pixel through two spectral threshold approaches applied to NIR and SWIR2 bands. NDVI trends from 2019 to 2023, show higher greenness NDVI up to 0.5 in the wetland compared to the surrounding area. These variations are influenced by seasonal harvesting, drought years, and the warming trend. This study is crucial for water management in the Usangu wetland, which

serves as a vital source and watershed for the Ruaha River, supporting both ecological and agricultural sustainability in the region.

Keywords

Climate Change, Usangu Wetland, Land Surface Temperature (LST), Remote Sensing (RS), Land Use and Land Change (LULC), Water Indices, Normalised Difference Vegetation Index (NDVI)

1. Introduction

The relationship between Land Surface Temperature (LST), Normalized Difference Vegetation Index (NDVI), Standardized Precipitation Index (SPI), and precipitation is critical for understanding climate change (Gaikwad et al., 2022; Khan et al., 2018). Landsat and Sentinel imagery have been extensively used for climate analysis and hydrological studies over several decades, providing valuable insights into water resource management (Cheng et al., 2024; Hoai et al., 2025). The Usangu wetland, a significant water catchment within the Ruaha River hydrological system (Mwita, 2016), plays a vital role in regional water supply. However, research indicates a notable annual decline in the Ruaha River water flow, which adversely affects downstream socio-ecological systems (MOW, 2015). The Usangu Wetland is not a Ramsar site under the Convention on Wetlands (Kashaigili et al., 2006). Its conservation relies entirely on Tanzania's national policies and stewardship commitment, lacking international safeguards.

Remote Sensing (RS) techniques are widely recognized for their ability to evaluate water stress resulting from climatic variations, offering a robust framework for monitoring environmental changes. NDVI trend analysis is frequently employed to assess vegetation responses to climate change (Muhury et al., 2024), with studies demonstrating a strong linear correlation between NDVI and climate change impacts (Zhang et al., 2024). LST serves as a key indicator of the energy balance between land surfaces and water bodies (Song et al., 2025), and its variations are closely tied to topographic factors, land cover, and vegetation indices. Literature suggests that NDVI fluctuations are influenced by both climate change and anthropogenic activities (Tuoku et al., 2024). LST significantly impacts NDVI variations due to energy imbalances (Karnieli et al., 2010; Xu et al., 2011). Latitude and altitude variations further affect vegetation growth, with a negative LST-NDVI relationship associated with altitude often indicating soil water stress and increased evapotranspiration rates (Nemani & Running, 1997; Stisen et al., 2007).

Monitoring water presence in wetlands like the Usangu wetland often involves indices such as Normalised Difference Water Index (NDWI), Modified Normalised Difference Water Index (MNDWI), Modified Normalised Difference Water Index 2 (MNDWI2), and the Water in Wetland (WIW) method (Acharya et al., 2018). For instance, a study on the Renuka wetland, a Ramsar site, utilized the

Normalized Difference Water Index (NDWI) through Google Earth Engine (GEE) to map water bodies using Landsat imagery. NDWI effectively identifies water distribution, even in areas with minimal vegetation. The WIW method (Lefebvre et al., 2019) provides a comprehensive RS approach for detecting water in vegetated regions, leveraging Near Infrared (NIR) and Short-Wave Infrared 2 (SWIR2) bands, making it adaptable across diverse vegetation types.

2. Materials and Methods

Study Area

The Usangu wetland, located in Mbarali District, Mbeya Region, Tanzania, lies between latitudes 7˚45'S to 9˚00'S and longitudes 33˚40'E to 35˚00'E and consist of five subsystems (Franks, 2003). The Usangu wetland is the study area within Mbarali District, though its hydrological influence extends slightly beyond, including the riparian reach through the Ruaha National Park and the Mtera/Kidatu hydroelectric system. The Usangu sub-catchment drainage area spans approximately 20,800 km^2, with 4840 km^2 (23% of the plains) situated below 1100 m above mean sea level (msl), while the remaining 77%, representing the higher catchment, ranges from 1100 m to 2000 m above msl (Hyandye & Martz, 2017).

The Usangu Plains as shown in **Figure 1** and **Figure 2** consist of western and eastern wetlands connected by the Great Ruaha River, with other major perennial rivers draining the plains, including the Mbarali, Kimani, Chimala, and Ndembera (Kashaigili et al., 2006). Smaller rivers, such as the Umrobo, Mkoji, Lunwa, Mromboji, Ipatagwa, Mambi, Kioga, Mjenje, Kimbi, Itumbo, and Mswiswi, also contribute to the drainage network. The plains feature extensive alluvial deposits that support irrigation, livestock keeping, and dryland farming, as illustrated in **Figure 3**. In the Usangu wetland, mean rainfall ranges from 500mm to 700mm, and mean annual temperature ranges from 18˚C to 28˚C (Thomas et al., 2024). The wetland's outflow sustains the Ruaha National Park, providing essential ecosystem services for wildlife conservation, serves as a water source for the Kidatu Dam, and contributes approximately 15% to the 4 million capacity Stigler Gorge Hydro Power Dam (Franks et al., 2004).

3. Methodology

Wetland areas condition was assessed using 30m SRTM DEM, SPI (PERSIANN-CDR/CHIRPS), LST (Landsat/Sentinel-2), WIW, NDVI (MODIS), NDWI/MNDWI. Validation of the CHIRPS data done using historical CMIP6. The datasets used in analysis and their processing are listed in **Table 1**.

3.1. SPI Data

The precipitation dataset sourced from the Climate Data Record (CDR) of NOAA PERSIANN, which is accessible through the cloud-based Google Earth Engine (GEE) platform using JavaScript API code. This dataset has a spatial resolution of 0.25 degrees. The dataset was clipped and filtered to match the wetland area. The

Standardized Precipitation Index (SPI) was calculated to assess temporal and spatial patterns of drought and wet conditions, with SPI values ranging from -3 (extreme drought) to 2 (extreme wet). For visualization, a timeseries plot was generated to examine the temporal consistency of SPI across the study period (as shown in Figure 11). Spatial consistency was validated by comparing SPI with precipitation clustering, derived using the K-Means algorithm, and presented in Figure 10.

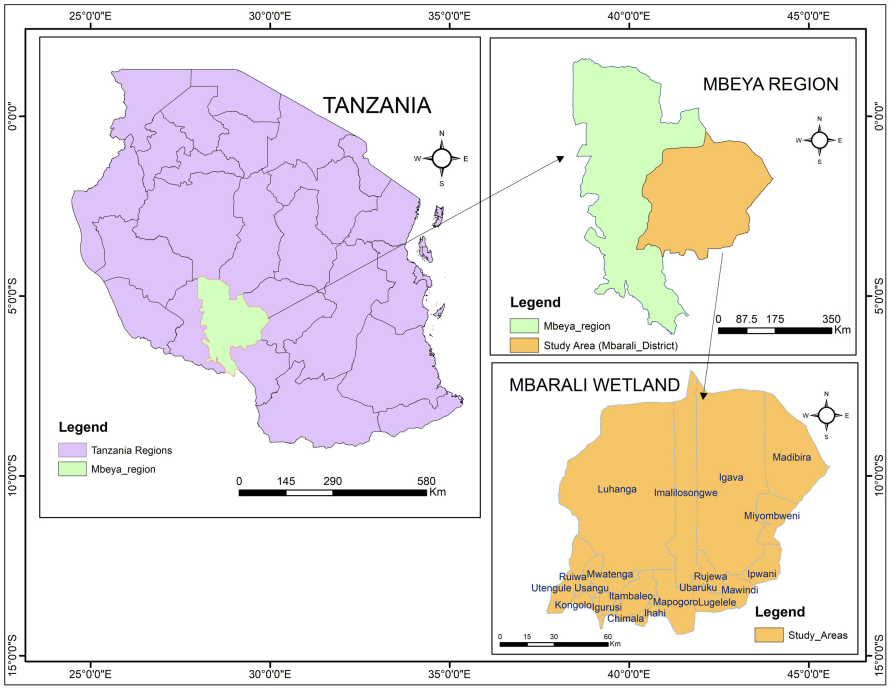

Figure 1. Usangu catchment map.

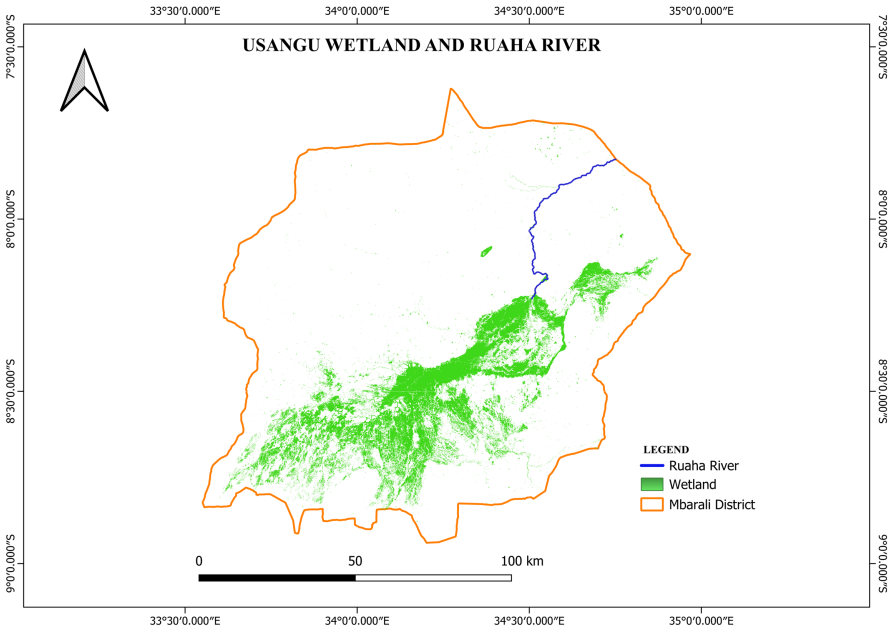

Figure 2. The wetland area.

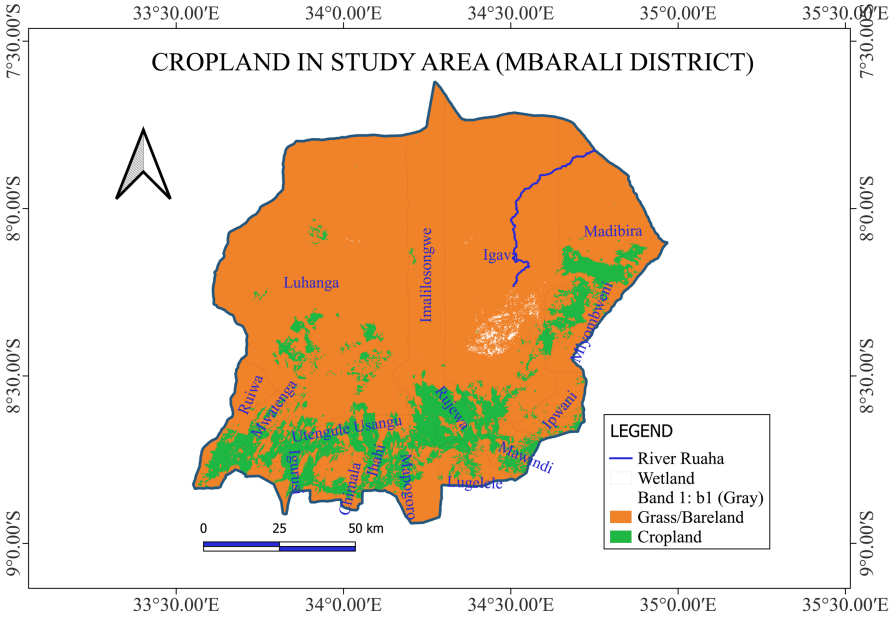

Figure 3. Cropland in the wetland area.

3.2. LST Data

Land Surface Temperature (LST) modelling for the Usangu wetland was conducted using thermal infrared bands ST_B10 from Landsat 8 and 9. The Landsat derived LST was then statistically compared to Sentinel-2 spectral bands (B2-B12) and topographic features elevation, slope and NASA SRTM Digital Elevation Model (DEM) data to predict high-resolution (10m) LST across the wetland, processed within Google Earth Engine (GEE). To ensure data quality, cloud filtering techniques were applied to mask clouds and generate cloud-free images, minimizing noise in the dataset for training and testing. The images were then processed using a median function to create composite images and cropped to fit the study area.

A Random Forest model was employed for LST prediction, trained using machine learning techniques with input features including spectral bands, vegetation indices, and elevation data derived from the SRTM DEM. The model was configured to use 70% of the dataset for training and 30% for testing. Model performance was evaluated by comparing the predicted LST to reference LST data, with errors quantified using the Mean Absolute Error (MAE). The relationship between reference and predicted LST was assessed through a linear correlation, visualized with a trend line and quantified using the Pearson correlation coefficient.

3.3. Precipitation Data

Precipitation data for the study area were sourced from the Climate Hazards Group InfraRed Precipitation with Station data (CHIRPS) dataset (Zhang et al., 2025), accessed as a spatial dataset via the cloud based Google Earth Engine (GEE) platform. The CHIRPS dataset provides a high spatial resolution of 0.05 degrees and consists of daily precipitation records, covering the analysis period since 1981 (Agha Kouchak et al., 2011). To examine trends, seasonal patterns, and residual

components in the precipitation data, statistical time series decomposition was performed using the Seasonal-Trend Decomposition using LOESS (STL) method (He et al., 2022; RB, 1990). The STL approach was selected for its ability to elucidate natural variability in precipitation data, aiding in the interpretation of trends, seasonal cycles, and time series characteristics, as well as identifying anomalies (He et al., 2022).

Coupled Model Intercomparison Project Phase 6 (CMIP6) historical precipitation data was bias corrected using CHIRPS observations via linear scaling (Lafon et al., 2013; Teutschbein & Seibert, 2012). The resulting time series **Figure 4** reveals severe dry spells (≤200 mm/month) in the Usangu wetland region during 2010-2015.

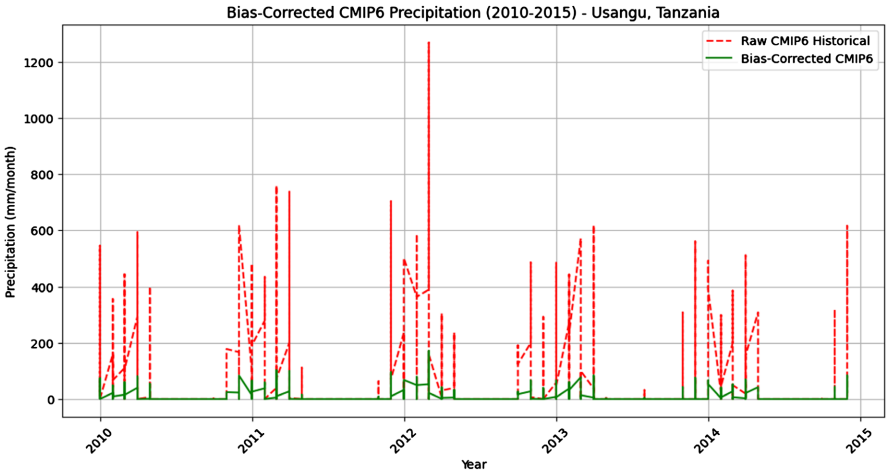

Figure 4. Bias corrected CMIP6 precipitation.

K-Means clustering of precipitation data was conducted using machine learning techniques within the GEE Python environment, as illustrated in **Figure 10** (Reddy et al., 2023) and equation 1. This process utilized geographical data from 299 satellite images obtained from the Global Precipitation Measurement (GPM) dataset, specifically NASA/GPM_L3/IMERG_MONTHLY_V07, which has a spatial resolution of 0.1 degrees. The GPM data, available monthly, spanned the period from 2000 to 2024. The K-Means algorithm was applied to categorize the precipitation data into four classes: Heavy, Moderate, High, and Low. A timeseries plot was generated to compare the classified precipitation data with the Standardized Precipitation Index (SPI) for validation.

$$J = \sum_{i=1}^{4} \sum_{x \in C_i}^{n} \left(x_n - \mu_i \right)^2 \quad (1)$$

C_i: Data points in cluster, μ_i: Mean (centroid) of cluster, x: Precipitation value.

3.4. NDVI Data

The Normalized Difference Vegetation Index (NDVI) data were sourced from the MODIS MOD13A1.061 product (Terra Vegetation Indices 16-Day Global 500 m), covering the period from 2019 to 2023 using equation 2. The NDVI data were

clipped to the wetland area. To improve data quality, the NDVI infrared bands were filtered to remove cloud cover and then multiplied by the appropriate scale factor provided in the MODIS dataset to enhance visualization. Monthly averages of NDVI were calculated for each year from 2019 to 2023 to capture temporal variations in vegetation health across the study period **Figure 13**.

$$\mathrm{NDVI} = (\mathrm{NIR} - \mathrm{RED})/(\mathrm{NIR} + \mathrm{RED}), \tag{2}$$

3.5. Visualization of MDWI, ANDWI, NDVI and WIW

Visualization of water conditions in the Usangu wetland was conducted using spectral indices, including the Normalized Difference Vegetation Index (NDVI), Modified Normalized Difference Water Index (MDWI), Normalized Difference Water Index (NDWI), Water in Wetland (WIW), and Automated Normalized Difference Water Index (ANDWI). The data were sourced from Landsat 8 Level 2 (surface reflectance) images, covering the period from 2020 to 2024. These images were filtered to include only those with less than 10% cloud cover to ensure data quality for the wetland area. A composite median image was derived from the surface reflectance bands of the filtered satellite images to reduce temporal variability and enhance consistency.

The NDVI map was generated in **Figure 15(a)** using the near-infrared (NIR) and red bands to assess vegetation health, calculated as NDVI = (NIR − Red)/(NIR + Red). To detect water amidst the wetland complex vegetation cover, multiple water indices were employed, leveraging various spectral bands. NDWI, as described in prior studies (Ashok et al., 2021; Laonamsai et al., 2023; Xu, 2006), was calculated using the NIR and green bands to identify water bodies. The MDWI (Laonamsai et al., 2023) utilized the short-wave infrared (SWIR) band alongside the green band to enhance water detection in vegetated areas. The WIW index method (Lefebvre et al., 2019) was applied using surface reflectance bands in the NIR and SWIR ranges, incorporating a logical thresholding approach to improve water detection reliability, particularly when other indices were less effective. The ANDWI (Rad et al., 2021) was computed using red, green, blue (RGB), NIR, and both SWIR1 and SWIR2 bands to improve water demarcation and visibility in vegetated wetlands.

$$\mathrm{NDWI} = \frac{(\mathrm{GREEN} - \mathrm{NIR})}{(\mathrm{GREEN} + \mathrm{NIR})} \tag{3}$$

$$\mathrm{MDWI} = \frac{(\mathrm{GREEN} - \mathrm{SWIR})}{(\mathrm{GREEN} + \mathrm{SWIR})} \tag{4}$$

$$\text{Water bodies} \approx 0.2 \quad \text{Vegetation} \approx\!< 0$$

$$\mathrm{ANDWI} = \frac{(\text{Visible Bands} + \mathrm{NIR}) - (\mathrm{SWIR1} + \mathrm{SWIR1} + \mathrm{SWIR2})}{(\text{Visible Bands} + \mathrm{NIR}) + (\mathrm{SWIR1} + \mathrm{SWIR1} + \mathrm{SWIR2})} \tag{5}$$

$$\mathrm{wiw} = (\mathrm{nir} \le 0.1735) \,\&\, (\mathrm{swir2} \le 0.1035) \tag{6}$$

$$\mathrm{wiw} = (\mathrm{nir} \le 0.1735) \,\mathrm{or}\, (\mathrm{swir2} \le 0.1035) \tag{6a}$$

Table 1. Description of dataset.

Dataset	Description	Year	Source
DEM	Digital Elevation Model data used to analyse elevation impacts on LST and other variables, with a spatial resolution of 30 m.	2024	NASA SRTM (Shuttle Radar Topography Mission) DEM, accessed via Google Earth Engine (GEE).
SPI	Standardized Precipitation Index calculated to assess drought and wet conditions, derived from daily precipitation data with a spatial resolution of 0.25 degrees.	2000-2024	NOAA PERSIANN-CDR (Climate Data Record), accessed via Google Earth Engine (GEE) (Chang et al., 2022).
LST	Land Surface Temperature data used to model temperature variations and their impacts on water and vegetation, derived from thermal infrared bands with a resolution of 30 m.	2020-2024	Landsat 8 TIRS and predicted with indices from Sentinel-2 Level 2A, processed via Google Earth Engine (GEE).
WIW	Water in Wetland index used to detect water pixels in vegetated areas, leveraging NIR and SWIR bands with logical thresholds, applied to map water extent.	2020-2024	Landsat 8 Level 2 and Sentinel-2, processed via Google Earth Engine (GEE) (Lefebvre et al., 2019).
NDVI	Normalized Difference Vegetation Index used to assess vegetation health, derived from NIR and red bands, with a spatial resolution of 500 m.	2019-2023	MODIS MOD13A1.061 (Terra Vegetation Indices 16-Day Global 500m), accessed via Google Earth Engine (GEE).
NDWI	Normalized Difference Water Index used to detect water bodies, calculated using green and NIR bands, applied to map water distribution in the wetland.	2020-2024	Landsat 8 Level 2, processed via Google Earth Engine (GEE).
MDWI (MNDWI)	Modified Normalized Difference Water Index, a variant of NDWI using SWIR bands (e.g., SWIR2), applied to enhance water detection in vegetated areas.	2020-2024	Landsat 8 Level 2, processed via Google Earth Engine (GEE) (Bourletsikas et al., 2023; Laonamsai et al., 2023).
Precipitation (CHIRPS)	Daily precipitation data used for trend analysis and SPI calculation, with a spatial resolution of 0.05 degrees.	1981-2024	Climate Hazards Group InfraRed Precipitation with Station data (CHIRPS), accessed via Google Earth Engine (GEE) (Zhang et al., 2025).
Precipitation (GPM)	Monthly precipitation data used for K-Means clustering to classify precipitation patterns, with a spatial resolution of 0.1 degrees.	2000-2024	NASA/GPM_L3/IMERG_MONTHLY_V07 (Global Precipitation Measurement), accessed via Google Earth Engine (GEE) (Reddy et al., 2023).

4. Results

4.1. Land Surface Temperature (LST)

Studies show that rivers drain approximately 75% of the surface water on land, underscoring the critical role of river systems in wetland hydrology (Bourletsikas et al., 2023). In agricultural regions, land surface emissivity has been identified as a crucial factor for energy balance, influencing thermal dynamics in such areas (Das et al., 2021). Also, research has demonstrated that Land Surface Temperature (LST) significantly affects surface water temperature and river flow, with higher LST values often leading to increased water temperatures and altered flow patterns (Lefebvre et al., 2019). These findings from other regions provide a comparative framework for interpreting the hydrological and thermal dynamics observed in the Usangu wetland **Figure 5**.

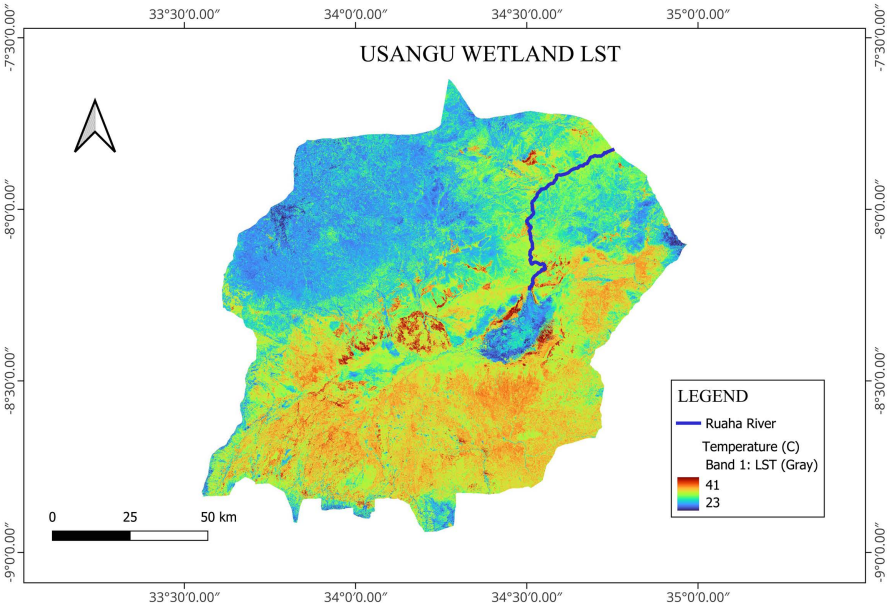

Figure 5. LST spatial variation in the study area.

The linear regression r value of 0.789 in the correlation of LST reference against prediction in **Figure 6** suggests that the temperature values are significantly captured. The wetland ecosystem is positively affected by the LST due to an imbalance of the energy (Xu et al., 2011). The regression line data points exhibit significant clustering between 20˚C and 30˚C. The alteration in Land Surface Temperature (LST) trends has affected land cover changes, desertification, and water management. **Figure 7** illustrates the area influenced by the increase in LST within the basin.

The r correlation in **Figure 7** illustrates the MDWI (Modified Normalized Difference Water Index) spectral index, which indicates that water detection is lower than that of MNDWI, which indicates the availability of water in the wetland but is obscured by vegetation. According to the Histogram, the correlation results in the wetland exhibit identical greenness and dryness values. The negative correla-

tion between the LST and elevation in Figure 8 indicates that there is opposite relationship between the two variables. Consequently, the wetland is characterized by a higher temperature than the rest of the areas as shown in Figure 5.

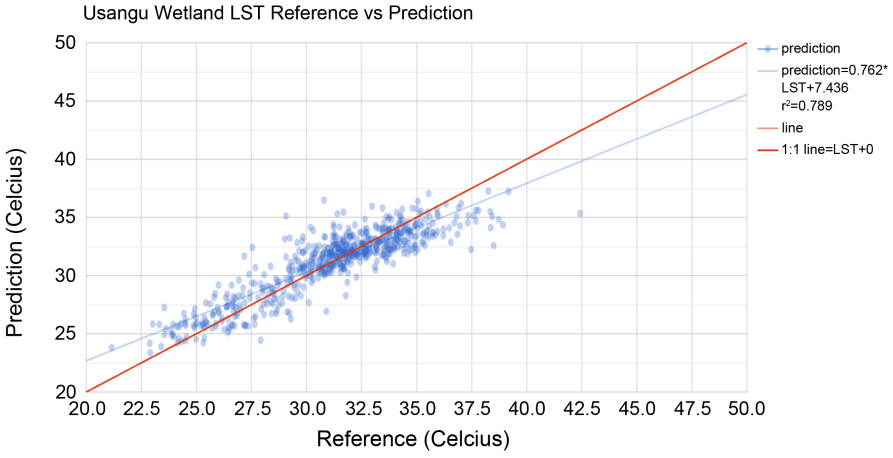

Figure 6. LST baseline (Reference) against prediction.

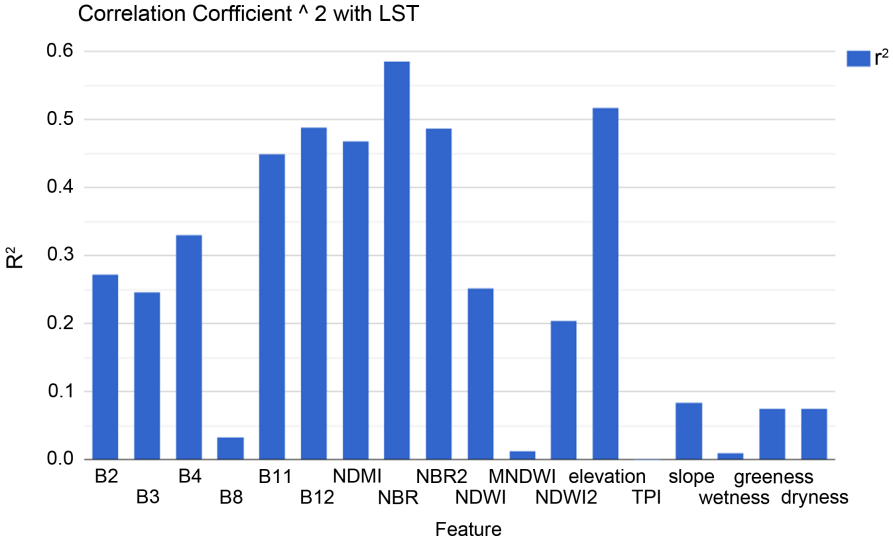

Figure 7. Correlation coefficient with LST.

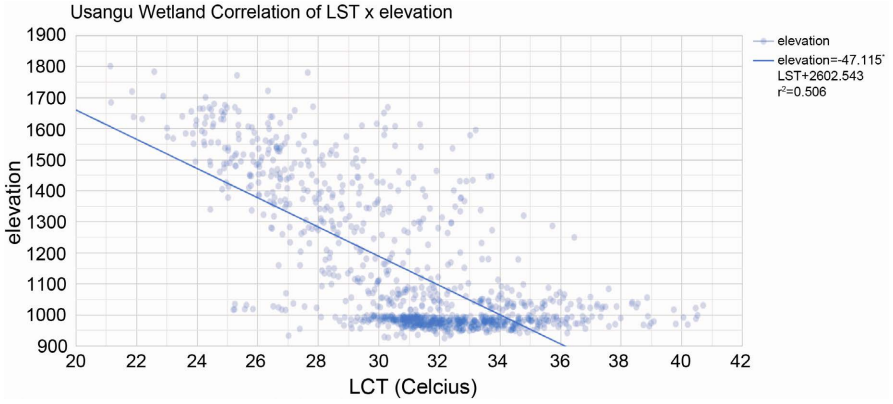

Figure 8. LST against elevation.

4.2. Precipitation

4.2.1. STL

The precipitation data was analysed using the ML of the stats model in the statistics package. The analysis of the trend indicates a long-term increase in precipitation from the 1990s to the 2020s, characterized by below-average levels in the 1990s and subsequent growth in the 2000s. The timeseries decomposition Figure 9 indicates years below the average from 2000 to 2003 and from 2010 to 2012. This timeframe aligns with the SPI Figure 11 depicting the dry spell in the wetland area.

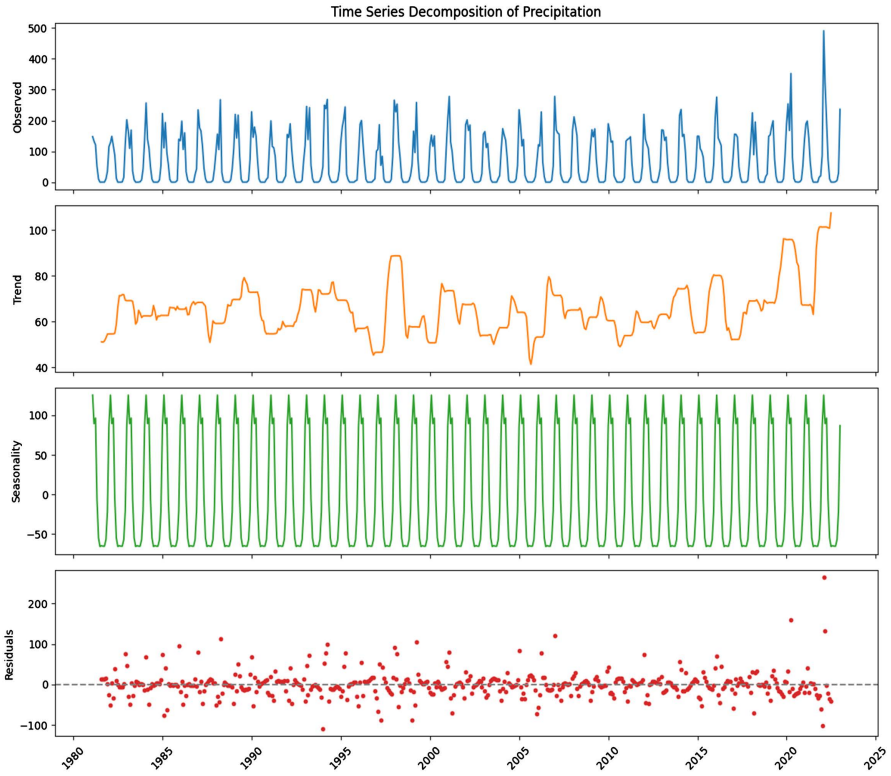

Figure 9. Timeseries decomposition of precipitation.

4.2.2. Standard Precipitation Index (SPI) in the Wetland Area

In K Means, the precipitation data categorised into four classifications: heavy (red), high (orange), low (blue), and moderate (green) as depicted in Figure 10. The years characterised by moderate precipitation, correlated with the SPI, are predominantly represented by green bars (moderate) and exhibit fewer red, orange, and blue bars: 2003, 2008, 2013, 2017, and 2023. Mean precipitation during the years with moderate rainfall in the study area is 731 mm. We selected 4 clusters to capture the meteorological significance of precipitation intensity distribution, achieving a silhouette score of 0.695 despite it being a lower score for the two clusters and three clusters.

The index indicates a long-term deficiency in rainfall. Figure 11 illustrates extended droughts occurring in the years 2003, 2008, 2013, 2017, and 2023. The SPI drought trend of the data is compared with Figure 9, which represents the precipitation dataset using K-Means.

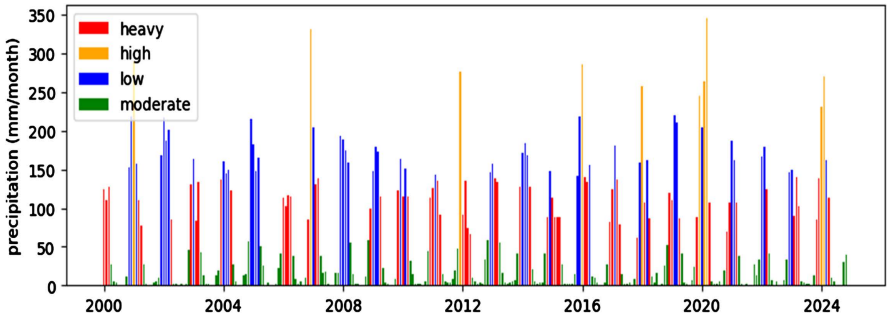

Figure 10. K-means precipitation temporal clustering.

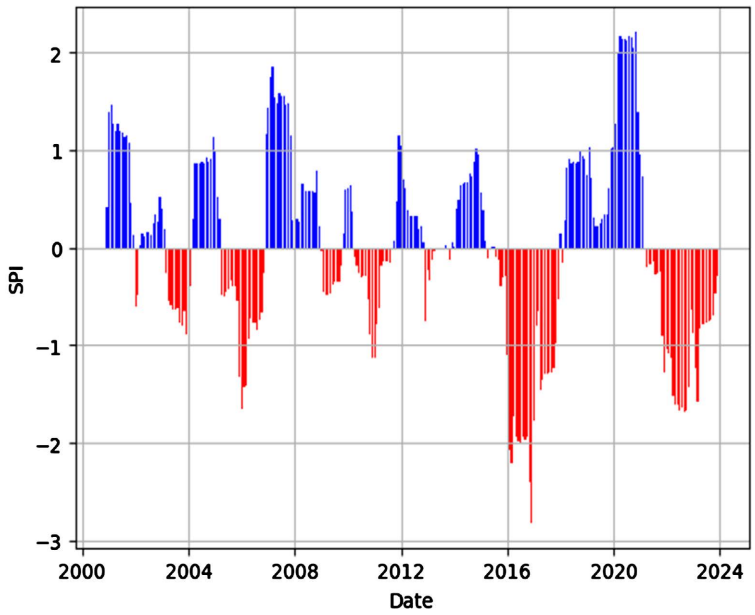

Figure 11. Standardized precipitation index (SPI) with drought years.

4.3. NDVI of the Vegetation Cover

The Usangu wetland, an agricultural area characterized by extensive irrigation development, experiences a drop in NDVI from April to May, coinciding with the paddy harvesting season. This seasonal decline explains the negligible correlation between drought anomaly years in the SPI index (shown in Figure 11) and NDVI values in the wetland in Figure 13. For instance, the drought year 2023 had a mean NDVI of 0.50, reflecting minimal impact. NDVI exhibits a decreasing annual trend from April to October, coinciding with rising LST in the study area shown in Figure 14, which peaks during this period. The NDVI map Figure 12 further illustrates the spatial distribution of vegetation across the region.

NDVI and NDWI of the Wetland

The NDVI Figure 15(a) indicate that the wetland is covered with healthy vegetation, with the maximum positive NDVI reaching 0.5. Normalised Difference Water Index (NDWI) (Xu, 2006) Figure 15(b) indicates a maximum negative value of −0.25, suggesting that the wetland is vegetated but deprived of water.

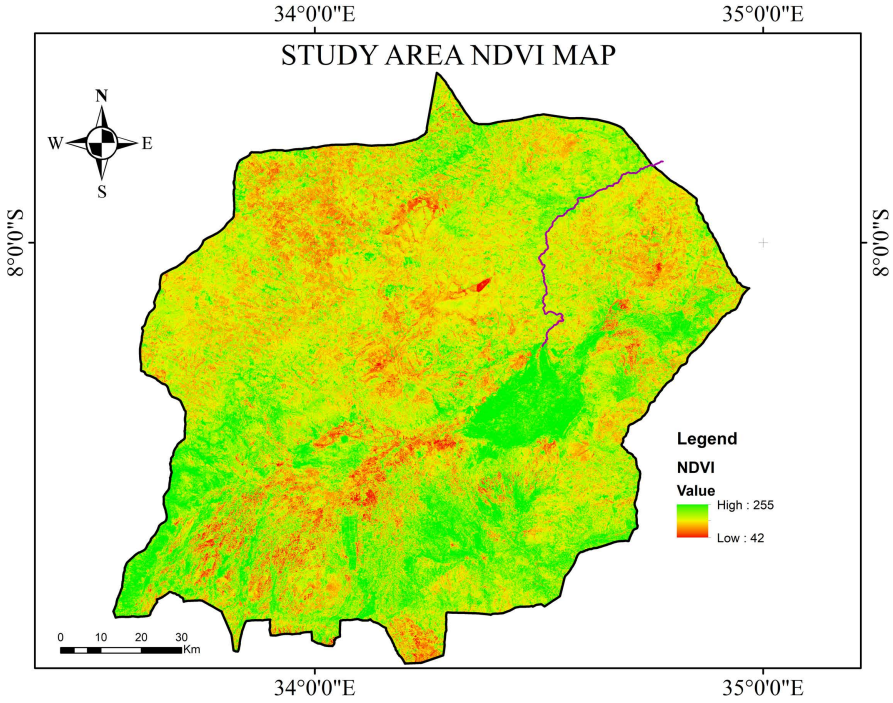

Figure 12. NDVI map showing spatial variation in the wetland area.

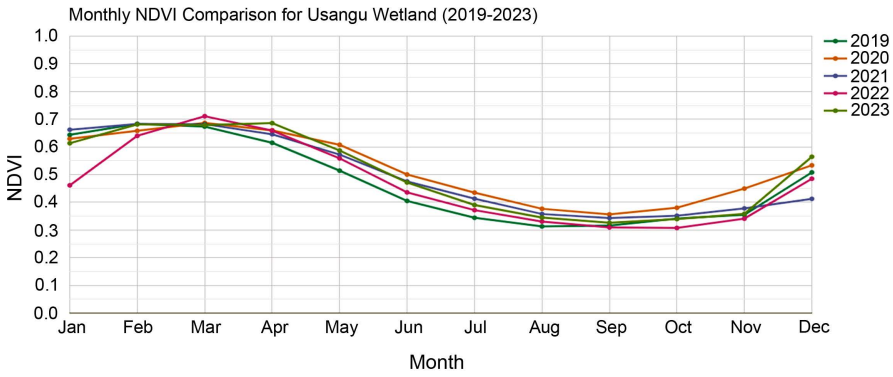

Figure 13. NDVI values show seasonal changes in vegetation health across the wetland throughout the year.

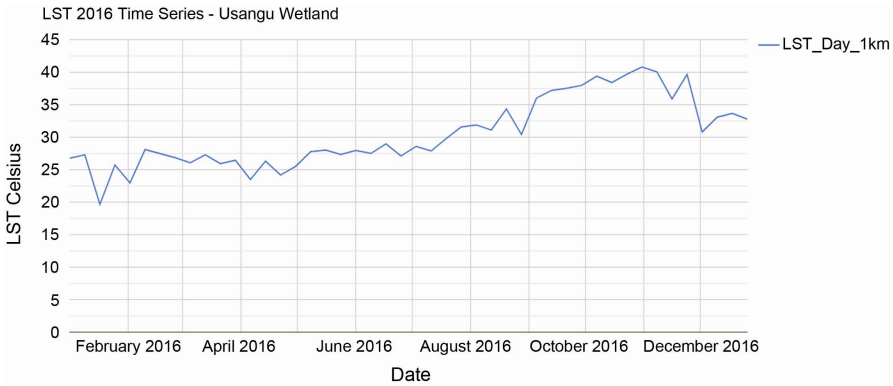

Figure 14. LST show seasonal changes in temperature across the wetland area throughout the year NDWI.

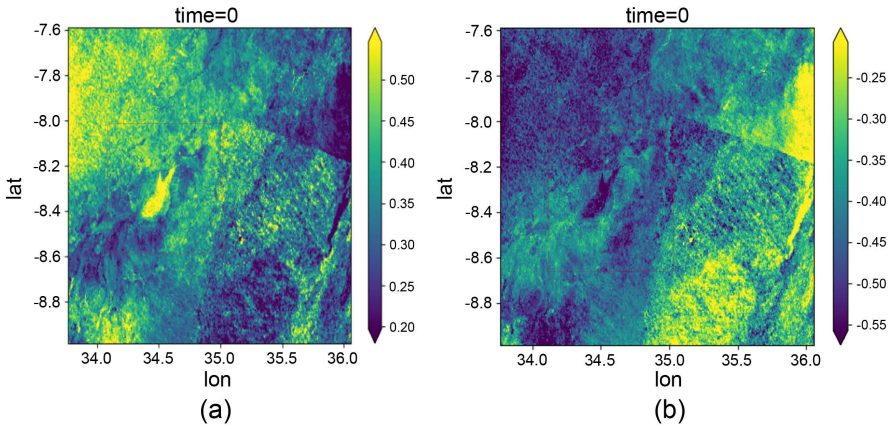

Figure 15. (a) Usangu Wetland NDVI; (b) Usangu Wetland NDWI.

4.4. Analysis of Water Availability in the Wetland Using ANDWI

The Modified Normalized Difference Water Index (MDWI) (Acharya et al., 2018), a variant of the Normalized Difference Water Index (NDWI) that incorporates the SWIR2 band, was applied to assess water and vegetation dynamics in the Usangu Wetland. Analysis of Figure 17(a) (ANDWI) and Figure 17(b) (NDWI) indicates water index values between −0.6 and −0.3, suggesting mostly non-water features within the wetland, as shown in Figure 16. This range of values, particularly the prevalence of negative NDWI values, indicates that the wetland areas are characterized by healthy vegetation, as negative values typically reflect higher vegetation presence due to the influence of the SWIR2 band in reducing water detection sensitivity in vegetated regions.

4.5. Water in Wetland Method (WIW)

The Water in Wetland (WIW) approach (Lefebvre et al., 2019), using single spectral bands from Landsat and Sentinel data alongside logical thresholds, was used to identify water pixels in the wetland area. Figure 18(a) and Figure 18(b) indicate that this methodology identified water pixels, hence demonstrating the presence of water

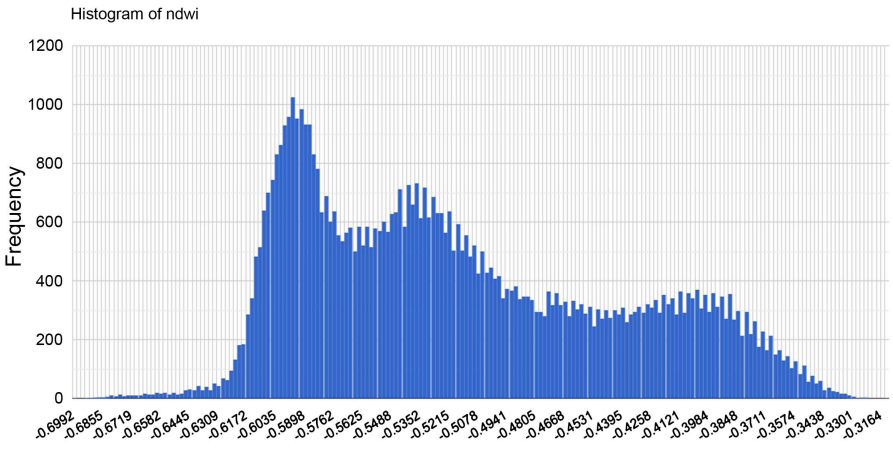

Figure 16. Histogram of wetland NDWI.

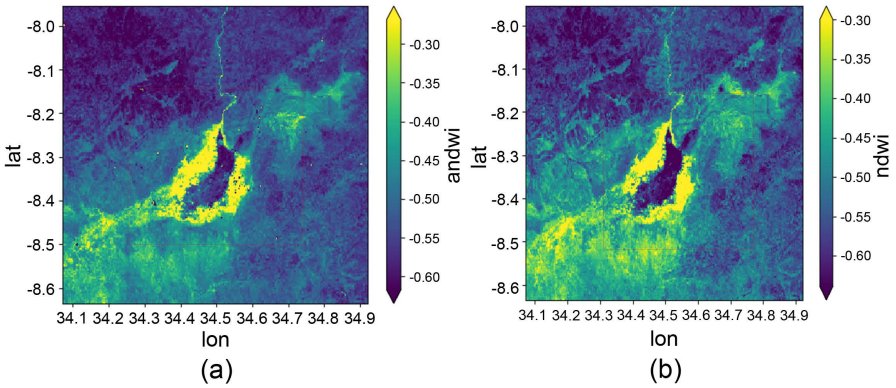

Figure 17. (a) ANDWI values in wetland indicate water coverage in the study area; (b) NDWI values in the wetland.

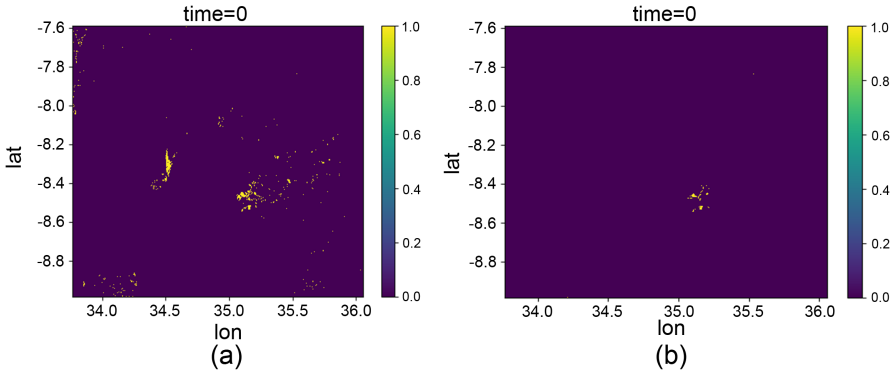

Figure 18. (a) WIW values using a relaxed classification logic, show the pixel-based water extent in the wetland study areas; (b) WIW values using a restricted classification logic, show the pixel-based water extent in the wetland study areas.

bodies within the wetland. Subsequent analysis in Figure 18(a) reveals an increased pixel density, signifying that the WIW method with moderate logical criteria detected a greater concentration of water pixels in contrast to a more restrictive approach in Figure 18(b).

The Water in Wetland (WIW) method employs spectral thresholds applied to Near-Infrared (NIR) and Short-Wave Infrared 2 (SWIR2). Two distinct logical conditions govern water detection. The stricter condition equation 6 requires both thresholds to be satisfied simultaneously and is best suited for mapping permanent water bodies where precision is critical. The relaxed condition equation 6a requires at least one threshold to be satisfied and is best suited for wetland delineation where omission errors must be minimised.

5. Conclusion

The presented analysis of the wetlands condition, including WIW, NDVI, LST, and SPI, can be applied for various purposes such as water resource management, biodiversity conservation and agricultural planning.

A statistically significant warming trend in the study area, as indicated by rising LST values, poses a risk to wetland management. Higher temperatures may in-

crease evaporation rates, reduce water availability, and stress the wetland ecosystem.

A decrease in greenness, reflected by declining NDVI values across multiple spectral bands, suggests a reduction in vegetation health within the wetland. This decline negatively impacts biodiversity by reducing habitat quality and food availability for wetland species.

The negative correlation coefficient (r) between LST and Digital Elevation Model (DEM) values directly affects the wetland. This negative correlation, as noted in Figure 8, indicates that lower elevations experience higher temperatures. Since the wetland is situated at lower elevations where water accumulates, as supported by the WIW analysis, this warming trend exacerbates heat stress in the wetland, potentially leading to increased evaporation and reduced water levels, which further threatens the ecosystem.

Indicators derived from wetland analysis, including Land Surface Temperature (LST), Standardized Precipitation Index (SPI), vegetation indices (NDVI), and water indices (MNDWI, NDWI, WIW), provide critical data for future environmental planning in the region. However, comprehensive Land Use/Land Cover (LULC) analysis is required to identify specific threats to wetland sustainability under prevailing trend of the Climate Change.

Acknowledgements

We acknowledge NASA/USGS for providing the Landsat satellite images used in this study. We also thank the Department of Earth and Climate Science of the University of Nairobi for the technical editing of this manuscript.

Conflicts of Interest

The authors declare no conflicts of interest regarding the publication of this paper.

References

Acharya, T. D., Subedi, A., & Lee, D. H. (2018). Evaluation of Water Indices for Surface Water Extraction in a Landsat 8 Scene of Nepal. *Sensors, 18,* Article No. 2580. https://doi.org/10.3390/s18082580

AghaKouchak, A., Behrangi, A., Sorooshian, S., Hsu, K., & Amitai, E. (2011). Evaluation of Satellite-Retrieved Extreme Precipitation Rates across the Central United States. *Journal of Geophysical Research: Atmospheres, 116,* D02115. https://doi.org/10.1029/2010jd014741

Ashok, A., Rani, H. P., & Jayakumar, K. V. (2021). Monitoring of Dynamic Wetland Changes Using NDVI and NDWI Based Landsat Imagery. *Remote Sensing Applications: Society and Environment, 23,* Article ID: 100547. https://doi.org/10.1016/j.rsase.2021.100547

Bourletsikas, A., Proutsos, N., Michopoulos, P., & Argyrokastritis, I. (2023). Temporal Variations in Temperature and Moisture Soil Profiles in a Mediterranean Maquis Forest in Greece. *Hydrology, 10,* Article No. 93. https://doi.org/10.3390/hydrology10040093

Chang, M., Li, P., Li, Z., & Wang, H. (2022). Mapping Tidal Flats of the Bohai and Yellow

Seas Using Time Series Sentinel-2 Images and Google Earth Engine. *Remote Sensing, 14,* Article No. 1789. https://doi.org/10.3390/rs14081789

Cheng, Q., Xie, R., Wu, J., & Ye, F. (2024). Deep Learning-Based Spatiotemporal Fusion Architecture of Landsat 8 and Sentinel-2 Data for 10 M Series Imagery. *Remote Sensing, 16,* Article No. 1033. https://doi.org/10.3390/rs16061033

Das, N., Bhattacharjee, R., Choubey, A., Ohri, A., Dwivedi, S. B., & Gaur, S. (2021). Time Series Analysis of Automated Surface Water Extraction and Thermal Pattern Variation over the Betwa River, India. *Advances in Space Research, 68,* 1761-1788. https://doi.org/10.1016/j.asr.2021.04.020

Franks, T. R. (2003). *A Livelihoods-Grounded Audit of the Sustainable Management of the Usangu Wetland and Its Catchment (SMUWC) Project in Tanzania*.

Franks, T., Lankford, B., & Mdemu, M. (2004). Managing Water Amongst Competing Uses: The Usangu Wetland in Tanzania. *Irrigation and Drainage, 53,* 277-286. https://doi.org/10.1002/ird.123

Gaikwad, S. V., Vibhute, A. D., & Kale, K. V. (2022). Assessing Meteorological Drought and Detecting LULC Dynamics at a Regional Scale Using SPI, NDVI, and Random Forest Methods. *SN Computer Science, 3,* Article No. 458. https://doi.org/10.1007/s42979-022-01361-0

He, R., Zhang, L., & Chew, A. W. Z. (2022). Modeling and Predicting Rainfall Time Series Using Seasonal-Trend Decomposition and Machine Learning. *Knowledge-Based Systems, 251,* Article ID: 109125. https://doi.org/10.1016/j.knosys.2022.109125

Hoai, C. T., Thi Thanh Huong, N., & Thi Hong Diep, N. (2025). Application of Sentinel-2A/B and Landsat 9 Imagery in Vegetation Cover Assessment: A Case Study in Dak Glong and Krong No Districts, Dak Nong Province. *IOP Conference Series: Earth and Environmental Science, 1501,* Article ID: 012010. https://doi.org/10.1088/1755-1315/1501/1/012010

Hyandye, C., & Martz, L. W. (2017). A Markovian and Cellular Automata Land-Use Change Predictive Model of the Usangu Catchment. *International Journal of Remote Sensing, 38,* 64-81. https://doi.org/10.1080/01431161.2016.1259675

John Mwita, E. (2016). Monitoring Restoration of the Eastern Usangu Wetland by Assessment of Land Use and Cover Changes. *Advances in Remote Sensing, 5,* 145-156. https://doi.org/10.4236/ars.2016.52012

Karnieli, A., Agam, N., Pinker, R. T., Anderson, M., Imhoff, M. L., Gutman, G. G. et al. (2010). Use of NDVI and Land Surface Temperature for Drought Assessment: Merits and Limitations. *Journal of Climate, 23,* 618-633. https://doi.org/10.1175/2009jcli2900.1

Kashaigili, B. A., Mbilinyi, B. P., Yawson, D. K. et al. (2006). *Use of a Hydrological Model for Environmental Management of the Usangu Wetlands, Tanzania*. IWMI.

Kashaigili, J. J., Mbilinyi, B. P., Mccartney, M., & Mwanuzi, F. L. (2006). Dynamics of Usangu Plains Wetlands: Use of Remote Sensing and GIS as Management Decision Tools. *Physics and Chemistry of the Earth, Parts A/B/C, 31,* 967-975. https://doi.org/10.1016/j.pce.2006.08.007

Khan, J., Wang, P., Xie, Y., Wang, L., & Li, L. (2018). Mapping MODIS LST NDVI Imagery for Drought Monitoring in Punjab Pakistan. *IEEE Access, 6,* 19898-19911. https://doi.org/10.1109/access.2018.2821717

Lafon, T., Dadson, S., Buys, G., & Prudhomme, C. (2013). Bias Correction of Daily Precipitation Simulated by a Regional Climate Model: A Comparison of Methods. *International Journal of Climatology, 33,* 1367-1381. https://doi.org/10.1002/joc.3518

Laonamsai, J., Julphunthong, P., Saprathet, T., Kimmany, B., Ganchanasuragit, T., Chom-

cheawchan, P. et al. (2023). Utilizing NDWI, MNDWI, SAVI, WRI, and AWEI for Estimating Erosion and Deposition in Ping River in Thailand. *Hydrology, 10,* Article No. 70. https://doi.org/10.3390/hydrology10030070

Lefebvre, G., Davranche, A., Willm, L., Campagna, J., Redmond, L., Merle, C. et al. (2019). Introducing WIW for Detecting the Presence of Water in Wetlands with Landsat and Sentinel Satellites. *Remote Sensing, 11,* Article No. 2210. https://doi.org/10.3390/rs11192210

MOW (2015). *Rufiji Basin Integrated Water Resource Management Drainage-IWRMD Volume II.* https://www.google.com/search?client=firefox-b-d&q=Rufiji+Basin+IWRMD+Volume+II+2015%29+

Muhury, N., Apan, A., & Maraseni, T. (2024). Modelling Floodplain Vegetation Response to Climate Change, Using the Soil and Water Assessment Tool (SWAT) Model Simulated LAI, Applying Different GCM's Future Climate Data and MODIS LAI Data. *Remote Sensing, 16,* Article No. 1204. https://doi.org/10.3390/rs16071204

Nemani, R., & Running, S. (1997). Land Cover Characterization Using Multitemporal Red, Near-IR, and Thermal-IR Data from NOAA/AVHRR. *Ecological Applications, 7,* 79-90. https://doi.org/10.1890/1051-0761(1997)007[0079:lccumr]2.0.co;2

Rad, A. M., Kreitler, J., & Sadegh, M. (2021). Augmented Normalized Difference Water Index for Improved Surface Water Monitoring. *Environmental Modelling & Software, 140,* Article ID: 105030. https://doi.org/10.1016/j.envsoft.2021.105030

RB, C. (1990). STL: A Seasonal-Trend Decomposition Procedure Based on Loess. *Journal of Official Statistics, 6,* 3-73.

Reddy, C. S., Deepak Rao, N. S. K., Sisir, A., Srinivasa Raju, V. S., & Aravinth, S. S. (2023). A Comparative Survey on K-Means and Hierarchical Clustering in E-Commerce Systems. In *2023 International Conference on Intelligent Data Communication Technologies and Internet of Things (IDCIoT)* (pp. 805-811). IEEE. https://doi.org/10.1109/idciot56793.2023.10053472

Song, S., Shi, J., Fan, D., Cui, L., & Yang, H. (2025). Development of Downscaling Technology for Land Surface Temperature: A Case Study of Shanghai, China. *Urban Climate, 61,* Article ID: 102412. https://doi.org/10.1016/j.uclim.2025.102412

Stisen, S., Sandholt, I., Nørgaard, A., Fensholt, R., & Eklundh, L. (2007). Estimation of Diurnal Air Temperature Using MSG SEVIRI Data in West Africa. *Remote Sensing of Environment, 110,* 262-274. https://doi.org/10.1016/j.rse.2007.02.025

Teutschbein, C., & Seibert, J. (2012). Bias Correction of Regional Climate Model Simulations for Hydrological Climate-Change Impact Studies: Review and Evaluation of Different Methods. *Journal of Hydrology, 456-457,* 12-29. https://doi.org/10.1016/j.jhydrol.2012.05.052

Thomas, S., Richard, S. F., Andrew, T. K. P. R., Japhet, K. J., & Winfred, M. (2024). Analysis of Water Exchange Processes between Groundwater and Surface Water in the Usangu Plains, Tanzania. *Asian Journal of Environment & Ecology, 23,* 52-73. https://doi.org/10.9734/ajee/2024/v23i8584

Tuoku, L., Wu, Z., & Men, B. (2024). Impacts of Climate Factors and Human Activities on NDVI Change in China. *Ecological Informatics, 81,* Article ID: 102555. https://doi.org/10.1016/j.ecoinf.2024.102555

Xu, H. (2006). Modification of Normalised Difference Water Index (NDWI) to Enhance Open Water Features in Remotely Sensed Imagery. *International Journal of Remote Sensing, 27,* 3025-3033. https://doi.org/10.1080/01431160600589179

Xu, W., Gu, S., Zhao, X., Xiao, J., Tang, Y., Fang, J. et al. (2011). High Positive Correlation between Soil Temperature and NDVI from 1982 to 2006 in Alpine Meadow of the Three-River Source Region on the Qinghai-Tibetan Plateau. *International Journal of Applied Earth Observation and Geoinformation, 13,* 528-535. https://doi.org/10.1016/j.jag.2011.02.001

Zhang, H., Li, L., Zhao, X., Chen, F., Wei, J., Feng, Z. et al. (2024). Changes in Vegetation NDVI and Its Response to Climate Change and Human Activities in the Ferghana Basin from 1982 to 2015. *Remote Sensing, 16,* Article No. 1296. https://doi.org/10.3390/rs16071296

Zhang, J., Liu, Y., Zhang, B., Xiong, S., Wang, C., Wu, S. et al. (2025). Spatiotemporal-grained Quantitative Assessment of Construction-Induced Deformation along the MTR in Hong Kong Using MT-InSAR and Iterative STL-Based Subsidence Ratio Analysis. *International Journal of Applied Earth Observation and Geoinformation, 136,* Article ID: 104342. https://doi.org/10.1016/j.jag.2024.104342